



Chip-Scale Electrochemical Differentiation of SAM-Coated Gold Features Using a Probe Array

Michal Tencer,^{a,b,z} Anthony Olivieri,^a Bora Tezel,^a Heng-Yong Nie,^c and Pierre Berini^{a,d,z}

^aSchool of Electrical Engineering and Computer Science, University of Ottawa, Ottawa, Ontario K1N 6N5, Canada

^bMST Consulting, Ottawa, Ontario, Canada

^cSurface Science Western, University of Western Ontario, London, Ontario N6G 0J3, Canada

^dDepartment of Physics, University of Ottawa, Ottawa, Ontario K1N 6N5, Canada

A method for chemically differentiating the surface of a set of small, closely-spaced, lithographically-defined Au features on a die, from another set of similar features intimately inter-dispersed, is described. The key enabler of the method is a standard electronics probe array adapted to carry out electrochemistry on the features. The probe array is used first to verify the electrical integrity of features and the quality of electrical contacts by measuring electrical resistance, then, in the presence of the electrolyte, simultaneously maintain one potential on one set of Au features and another potential on the other set in order to carry out desired electrochemical reactions. The technique was demonstrated on dies bearing 40 electrically isolated Au features (based on 5 μm wide stripes) accessed via 64 contact pads each 100×100 μm² in area. The array had 64 probes, of which 16 were maintained at a desorbing potential (-1.6 V vs. Ag/AgCl) and 48 at a stability potential (-0.3 V). The surface compositions were analyzed with time-of-flight secondary ion mass spectrometry by imaging ion fragments characteristic to the thiols forming SAMs, thereby validating the process.
© 2012 The Electrochemical Society. [DOI: 10.1149/2.087203jes] All rights reserved.

Manuscript submitted September 28, 2011; revised manuscript received November 15, 2011. Published January 10, 2012.

Certain lab-on-a chip (bio) sensor designs are based on differential signals and thus require chemical differentiation of the sensor elements. Chemical differentiation of small (~μm's) closely-spaced features is challenging mostly because any droplet which can be practically deposited will be much larger than the distance between the features. For instance, a sessile 0.1 μl water droplet on a hydrophobic surface would have a footprint with a diameter larger than 700 μm, and even larger on a hydrophilic surface or when using a low-energy solvent.¹

Previously we described two different methods of chemical differentiation of closely-spaced Au features. The first approach was based on exploiting strong interfacial forces between a liquid and a lyophilic "guide."^{1,2} The other involved toposelective electrochemistry^{3,4} which is applicable to any micron-scale structure that can be electrically isolated; this approach would be clearly preferable over the "guide" method if it were scalable. The selective electrochemistry approach is based on reductive desorption of a SAM⁴⁻¹¹ and was demonstrated on electrically isolated arms of a single plasmonic gold interferometer.³ Alternative techniques for "microspotting", such as contact microprinting¹² and dip-pen lithography,¹³ may also be viable for this purpose but require specialized, dedicated equipment and/or processes.

The purpose of this paper is to resolve scaling issues related to toposelective electrochemistry^{3,4} and to demonstrate the approach at the die level by simultaneously differentiating several Au features defined lithographically on a sensor chip. We apply time-of flight secondary ion mass spectrometry (ToF-SIMS) to identify thiol molecules deposited on Au features by detecting characteristic ion fragments from the surface (following previous work³), thereby validating the process.

The example sensor chip employed here bears an array of 8 Au Mach-Zehnder interferometers (MZIs), used in long-range surface plasmon polariton (LRSP) biosensing,² interleaved with an array of 8 straight Au waveguides, as shown in Fig. 1. The arms of the MZIs should be chemically differentiated using thiol-based self-assembled monolayers (SAMs) with different affinities toward the analyte. Fig. 1 shows the layout of the plasmonic sensor chip and the design of a single MZI. One way of scaling the process is to design the chip/wafer in such a way that all the west MZI arms on the chip (and/or on the wafer) are connected to one common metal trace, with all the east arms connected to another trace, such that the traces can be biased with appropriate potentials,¹¹ as proposed previously.³ However, this

approach is not viable when using existing designs, artwork and chip supplies. The alternative proposed herein involves adapting and using a probe array, of the type used in the microelectronics industry for wafer and die testing, to perform electrochemistry. The probes are divided into two sets connected to the two operating potentials of the process and used to prepare a chip with the layout of Fig. 1 in which all the west arms are covered with one SAM and all the east arms are covered with another SAM.

Voltage Drop Between Waveguides Through the Electrolyte

The electrochemical differentiation of the arms of an array of MZIs (Fig. 1) involves applying the desorbing potential (-1.6 V vs. Ag/AgCl) to one arm only of each MZI. As was shown previously for the case of a single MZI,³ if the potential of only one of the arms is controlled, the other one will assume practically the same voltage because the resistance and voltage drop are negligible when compared to those between each of these and the counter electrode, so both arms would undergo electrochemical desorption. Consequently, the potentials of both arms (in general of all Au features) must be actively controlled. However, if distances between the features to be differentiated is sufficiently large (several millimeters or more), it is enough if only the active potential is controlled.¹¹ Here, we have a large number of features distributed over the whole area of the die (6.5 × 3.8 mm²) and it is important to see what the resistances through the electrolyte are in this case.

The electrical resistance between any two parallel metal traces through an electrolyte with the specific resistance ρ can be estimated as^{3,14,15}

$$R = \frac{\rho}{\pi L} \left[\sinh^{-1} \frac{2L}{D} - \sqrt{1 + \left(\frac{D}{2L}\right)^2} + \frac{D}{2L} \right]^{-1} \quad [1]$$

where L and D are the length of the traces and the distance between them, respectively. Based on this equation, it was shown for the 4-electrode configuration of Fig. 2 that the through-electrolyte voltage drop between the arms of a single MZI is a small fraction to the total voltage drop (~0.03). For the 16 MZI arms and 8 straight waveguides on the chip shown in Fig. 1a, the situation differs, in that we must deal with a variety of distances between features. To simplify calculations with Eqn. 1 the x (i.e., east-west) coordinate of any MZI arm was assumed to be an arithmetic average between the coordinate of its most extreme point and that of a Y-junction (see Fig. 1). With this assumption the average distances on the chip are 340 μm between a

^z E-mail: michaltencer@hotmail.com; berini@site.uottawa.ca

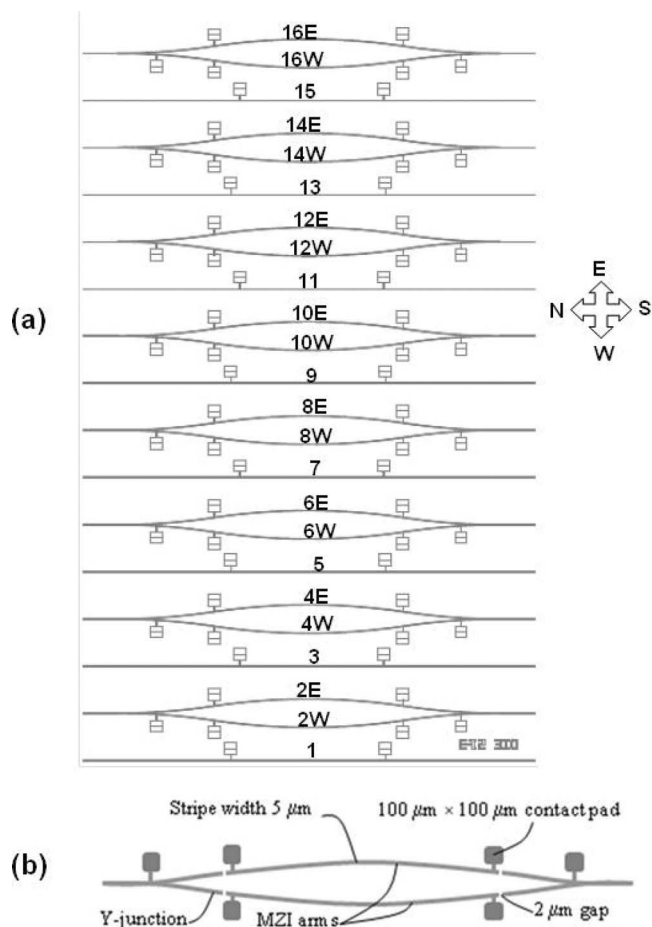


Figure 1. Plasmonic sensor chip featuring 8 Au MZIs and 8 straight Au waveguides formed from 5 μm wide 25 nm thick Au stripes with integrated contact pads and isolation gaps; (a) chip layout with waveguide numbering, **W** and **E** referring to the “West” and “East” arms of the MZIs; and (b) sketch of one MZI. There are 40 electrically-isolated Au features (each MZI has 2 Y-junctions and 2 arms, yielding 4 isolated features per MZI) accessed via 64 100×100 μm² contact pads (some are redundant).

straight waveguide and the nearest MZI arm and 120 μm between the east and west arms of any MZI. Using these coordinates, the distances between the first waveguide and any of the other ones are given in Table I, as well as the corresponding through-electrolyte resistances calculated using Eqn. 1.

Since both the measured and estimated resistance between the counter electrode and any of the waveguides is of the order of 1 MΩ, even with the furthest elements on the die, the resistance through the electrolyte (and the related voltage drop) between any pair of features is comparatively small. This is especially important given that electrochemical desorption of SAMs from non-textured (polycrystalline) Au happens over a potential range of 0.4 V. Thus, like with single MZIs, all the Au traces must be controlled with a potentiostat. With the probe array, this means that one set of the probes connecting to the west arms of all MZIs (Fig. 1a) should be connected to a desorbing potential of −1.6V (Ag/AgCl) and the other set connecting to all east arms, Y-junctions and straight waveguides should be maintained at a stabilizing potential, in this case −0.3 V (Ag/AgCl). Also, substrates which could provide a conductive path via tunneling (e.g., silicon with no protective oxide layer) should be avoided or the potentials compensated.⁴

The above considerations apply to a situation where the counter electrode is external to the die. However, it is conceivable to have both the counter electrode and the reference electrode microfabricated

Table I. Through-electrolyte resistance between Stripe #1 and other stripes on the die (numbered as in Fig. 1a) estimated using Eqn. 1; electrolyte resistivity $\rho = 1100 \Omega\text{m}$, stripe length = 3000 μm.

Stripe #	Distance μm	Resistance kΩ
2W	340	44.6
2E	460	49.9
3	800	63.5
4W	1140	76.0
4E	1260	80.3
5	1600	92.3
6W	1940	104.2
6E	2060	108.4
7	2400	120.3
8W	2740	132.2
8E	2860	136.4
9	3200	148.4
10W	3540	160.5
10E	3660	164.8
11	4000	177.0
12W	4340	189.2
12E	4460	193.5
13	4800	205.9
14W	5140	218.2
14E	5260	222.6
15	5600	235.1
16W	5940	247.6
16E	6060	252.1

onto the die, as is done in electrochemical sensing.¹⁶ In this case, the relative resistances discussed above will be different and maintaining independent control of both potentials may be less critical.

Experimental

Materials.— 1-Dodecanethiol (DDT), CH₃(CH₂)₁₁SH (≥98%, Arkema Inc.), Triethylene glycol mono-11-mercaptoundecyl ether (TPEG), HS(CH₂)₁₁(C₂H₄O)₃OH [C₁₇H₃₆O₄S], and potassium nitrate were purchased from Sigma-Aldrich Canada Ltd. De-ionized water was prepared from distilled water using a Zenopure Quatra 90LC system and the eluate with resistivity ≥ 17 MΩ cm was collected. 2-Propanol, semiconductor grade (Puranal) was obtained from Riedel-de Haën.

Sample preparation.— Both thiols were used as 2 mM solutions in 2-propanol. The dies, coated with a photoresist left over from the dicing process were first washed with acetone to remove the photoresist and then 2-propanol (to remove any acetone condensation products), rinsed with de-ionized water, dried and placed in a Novascan PSD-UV UV-ozone cleaner (5 min UV irradiation followed by 20 min ozone action). The dies were then immersed in the TPEG solution for 16 hrs, rinsed thoroughly with 2-propanol and water, and allowed to dry.

Substrates and structures.— The waveguide structures shown in Fig. 1 were defined from 25 nm thick, 5 μm wide Au stripes on a thin Cr adhesion layer, on a 15 μm thick thermally oxidized SiO₂ layer, on Si wafers, and were fabricated using lift-off and vacuum-evaporation.

Electrochemistry and electrical measurements.— Electrolysis experiments were performed with a Pine Research AFCBP1 bipotentiostat using a four-electrode configuration (one reference, two sets of working electrodes and one counter electrode), shown schematically in Fig. 2. The electrolyte was 0.1 M potassium nitrate. The counter electrode was a platinum wire coil. A double junction Ag/AgCl reference electrode was used. All potentials are reported

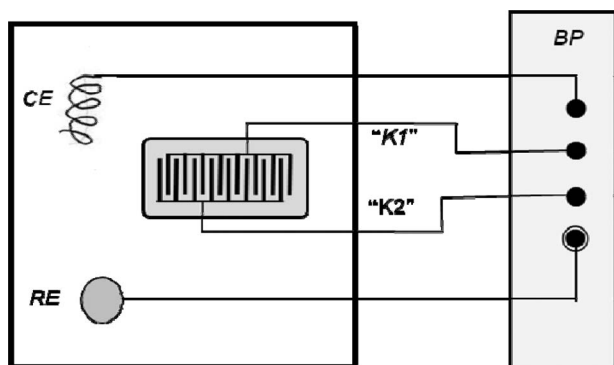


Figure 2. Four-electrode configuration for selective electrochemical desorption with a dual potential control: *BP* – Bipotentiostat, *K1* and *K2* – leads supplying the desorbing and stabilizing potentials, respectively, *CE* – counter electrode (platinum coil), *RE* – reference electrode.

with respect to this reference. DC resistances were measured with a Keithley 2000 multimeter.

Probe array card and cell.— The probe array shown in Fig. 3a consisted of a wafer tester FR-4 card adapted and manufactured by Accuprobe, Inc. (Salem, Mass., USA) according to our specifications. It featured 64 tungsten probes fixed on an epoxy ring whose coordinates matched those of the contact pads in Fig. 1a. No special material system was used for this prototype except that the bottom side was painted with a hydrophobic silicone varnish to minimize wetting by the electrolyte. Also, any shorting in dry or wet conditions was prevented by using plastic screws and isolation tape to mount the card to the metal bracket. The card was terminated with two ribbon cable connectors for communication with the outside world. The “electrochemical cell” (Fig. 3b) was a shallow container machined (carved) in a Macor glass ceramic tile, with additional cut-outs for the die, the reference electrode and counter electrode. On an optical table, the card was attached through a metal bracket to a 5-axis optical positioner bearing an additional goniometer, thus providing 6 degrees of freedom in total (*x-y-z*, *yaw-pitch-roll*). The ribbon cables were connected to a logical (electronic) switch matrix connected to both the bi-potentiostat and the multi-meter. The switch matrix was controlled using Labview as shown schematically in Fig. 4.

ToF-SIMS.— An ION-TOF (Gmbh) TOF-SIMS IV instrument equipped with a Bi liquid metal ion source was used to identify the thiols formed on the waveguide of the MZI. A 25 keV Bi_3^+ cluster primary ion beam with a pulse width of 24 ns (target current of ~ 1 pA) was used to bombard the sample surface to generate secondary ions from the surface. The secondary ions were extracted by an electric field (2 kV), mass separated, and detected via a reflectron type of time of flight analyzer. The cycle time for the processes of bombardment and detection was 100 μs , allowing parallel detection of ion fragments having a mass/charge ratio (*m/z*) up to 900 within each cycle. A pulsed, low energy (~ 18 eV) electron flood was used to neutralize sample charging. Only the negative secondary ion mass spectra were used because they are more informative than the positive ones in providing molecular ion fragments and their association with gold atoms (especially for DDT molecules).^{3,17,18} Secondary ion mass spectra were collected from 128×128 pixels over an area of $500 \times 500 \mu\text{m}^2$. The spectra were calibrated using H^- , C^- and Au_3^- . The mass resolution at CH^- and CH_3O^- were 2000 and 4000, respectively. Ion images were obtained by plotting the intensity of ion fragments characteristic to the thiols over the pixels. Because of the small size of the waveguide, for each area, in order to obtain good quality signals, ToF-SIMS data were collected by repeating 100 scans

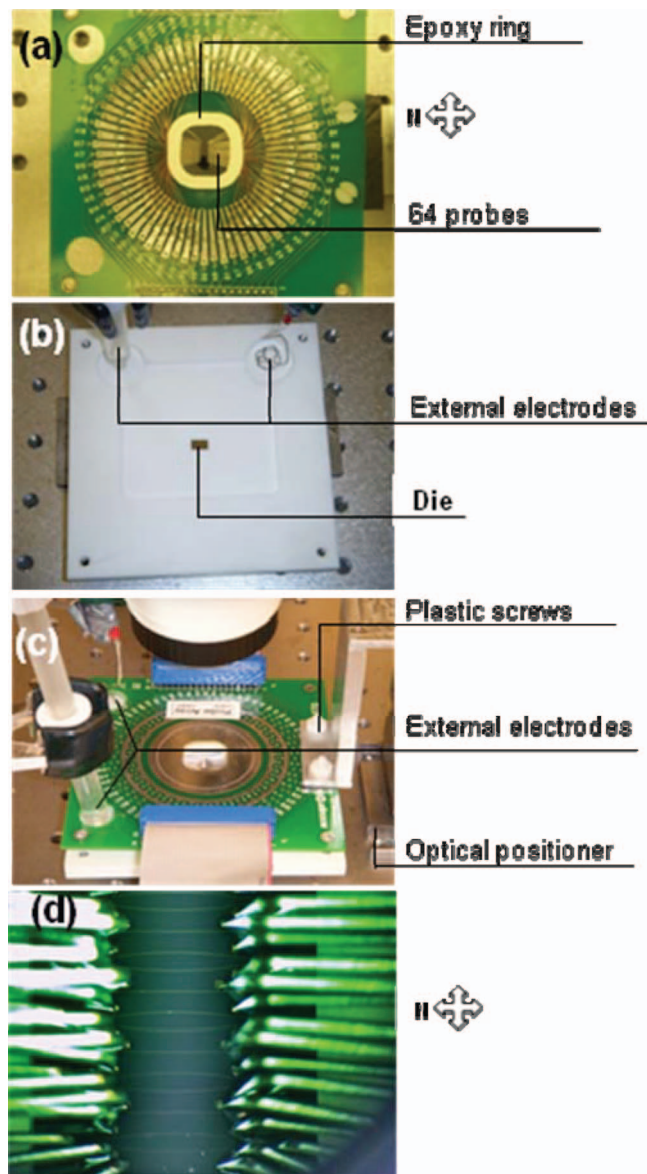


Figure 3. Probe array card and set-up: (a) bottom view of the card featuring the probes; (b) ceramic electrolytic cell; (c) full setup; (d) microscope image view of the die with probes contacting all contact pads.

over the area, with 5 shots of the primary ion beam per pixel in each scan.

Results and Discussion

Process.— As a result of a number of experimental attempts the following process proved suitable. The steps (A-J) below are related to process flow sketched in Fig. 5.

- The die is incubated with 2 mM TPEG in 2-propanol to produce SAM coated Au features, washed and dried as described previously.³
- The die is placed in the ceramic cell and the probe array is lowered over it using the optical positioner.
- The reference electrode and the counter-electrode are inserted into their positions in the ceramic cell through the cut-outs in the card, as shown in Fig. 3c
- Through Labview, the switch matrix is connected to the multi-meter.

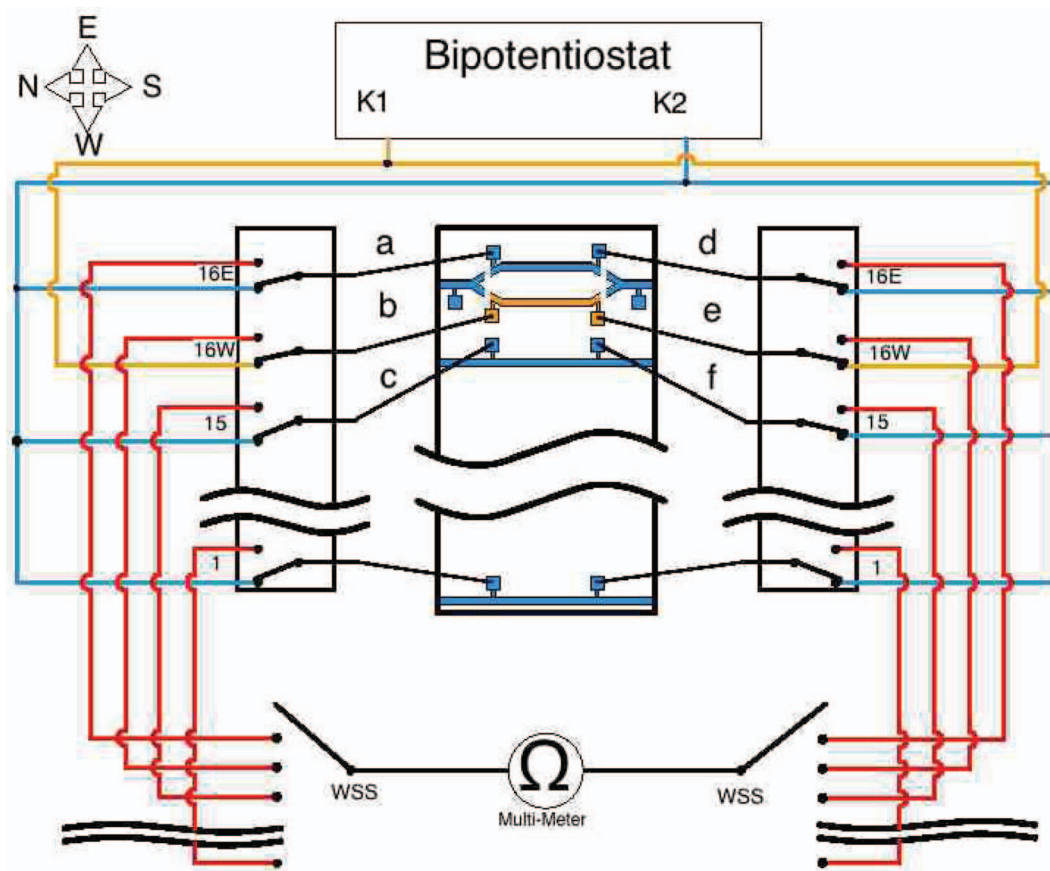


Figure 4. Schematic representation of the Labview-controlled electronic switch matrix; “a”-“f” denote pins assigned to contact pads on the die, K1 and K2 are the bi-potentiostat’s leads, WSS stands for waveguide selector switch.

- E. Using the positioner and a stereo microscope the probe array’s position is adjusted to make contact to all of the pads on the die simultaneously (Fig. 3d). After contacting, the electrical resistance between the probes assigned to the pads of each waveguide (24 in total; 16 MZI arms and 8 straight waveguides - Fig. 1a) were measured in quick succession and recorded. Achieving the expected resistance of ~ 1 k Ω for each verified both the electrical integrity of all waveguides and the quality of the probe to pad contacts.
- F. When the maximum number (preferably all) of contacts are achieved, the switch matrix is reconfigured with Labview to connect 16 probes contacting the pads of the west arms of the MZIs to the “K1” output lead of the bi-potentiostat and the remaining 48 probes (contacting the pads of the east arms and Y-junctions of MZIs and all of the straight waveguides) to the “K2” lead.
- G. The ceramic cell is filled with the 0.1 M KNO₃ electrolyte using the minimum amount necessary to wet the waveguides and ensure their through-electrolyte conductivity to both external electrodes.
- H. The bi-potentiostat is activated, with the “K1” lead set to -1.6 V and the “K2” lead to -0.3 V vs. Ag/AgCl for 5 seconds. This shorter^{3,4} (albeit sufficient) time was employed in order to complete the electrolysis before the capillary rise of the electrolyte along the probes deteriorates the electrical isolation between them.
- I. The die is removed from the cell, washed with water and 2-propanol.
- J. The die is incubated for 15 minutes in 2 mM DDT in 2-propanol. No noticeable SAM-thiol exchange occurs during that time.¹⁸ The die is washed in a jet of 2-propanol and submitted to analysis.

Dies and resistance measurements.— Results from two dies are reported here. One of the dies (Die 1) went through steps A through I, and the other die (Die 2) went through steps A through J, i.e., it was additionally exposed to a DDT solution (Fig. 5). Resistance values measured between the contact pads of all waveguides on two dies were measured as described in Step E of the process and are given in Table II. On one die (Die 1) one open was recorded (waveguide 8 E) while on the other die (Die 2) two opens were observed (8 E and 14W). An open was observed on 8 E over a large number of additional dies (with no exception) which suggests misalignment of one of the probes to a pad contacting this waveguide. On the other hand, the 14W open apparently is related to Die 2 specifically. The opens aside, the differences in the resistance values reflect most likely both small variations during the chip manufacturing process as well the quality of contact. Besides, multiple attempts to optimize the fit of the probe array and a die cause some damage to the contact pad.

Surface analysis.— The results of ToF-SIMS imaging of a die which went through the process flow of Fig. 5 are shown in Figs. 6 and 7. With Die 1 the last process step was I (no post-incubation with DDT). Fig. 6 shows Au and TPEG images of the bottom part of Die 1, which was constructed by stitching 13 images each of area $500 \times 500 \mu\text{m}^2$ taken across the chip. The upper row shows the Au image [represented by Au₃⁻ ion fragment (m/z 590.900)] displaying the outline of the Au arms and pads. Shown in the lower row is the image of CH₃O⁻ (31.020), representing TPEG. This ion fragment is the best among the characteristic ion fragments of TPEG, including C₂H₃O⁻ (43.020) and (C₂H₄O)₂OH⁻ (105.061),¹⁷ in terms of signal intensity and interference with other ion fragments. Some variability

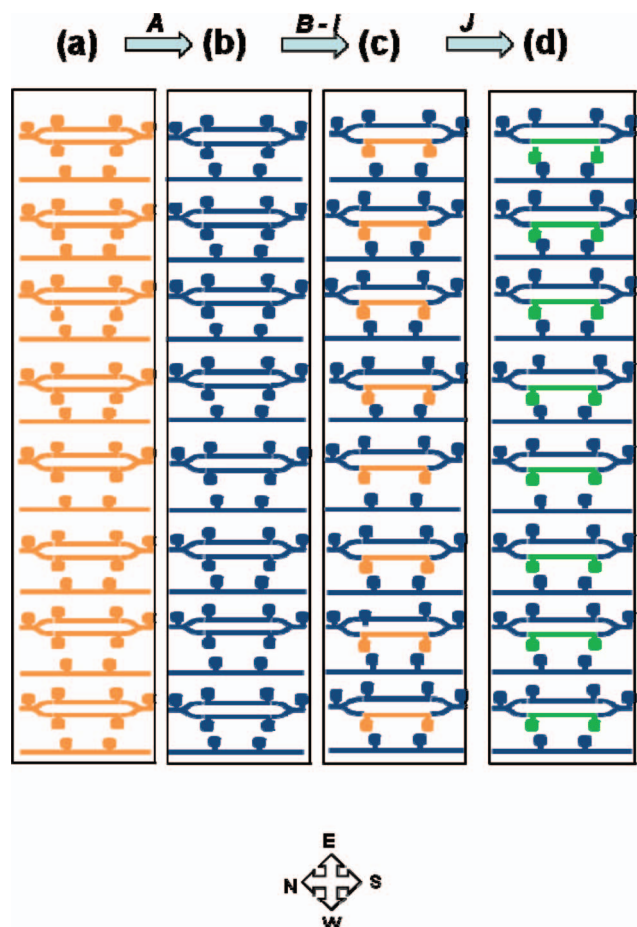


Figure 5. Process flow for the electrochemical differentiation of MZI arms; steps A - J are described in the text. (a) All Au surfaces are bare (gold). (b) TPEG SAM on all Au surfaces (dark blue). (c) TPEG SAM removed from all west arms of MZIs. (d) DDT SAM (green) on all west arms of MZIs.

in Au ion intensity can be seen, and are explained as follows. Firstly, some pads had to be contacted several times before the expected dry resistances were achieved (step E of the process), which might have damaged the thin Au layer forming the pads. Secondly, the signal contrast was optimized for each individual image (of area $500 \times 500 \mu\text{m}^2$) which may cause contrast variations between constituent images.

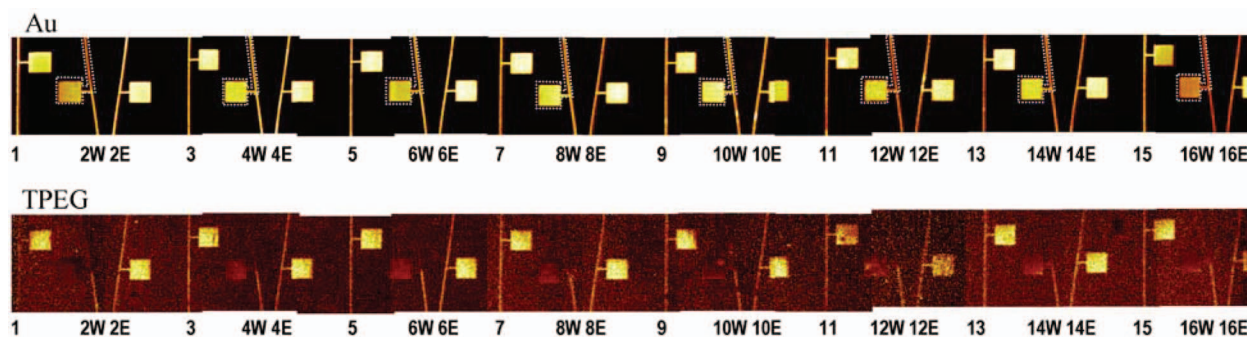


Figure 6. ToF-SIMS imaging of the South part of Die 1 subjected to process steps A-I (no DDT post-incubation). The images are created by stitching 13 separate $500 \times 500 \mu\text{m}^2$ images taken over all MZIs on the die. The upper image derived from Au_3^- ions shows the outline of the Au structures. The bottom image derived from CH_3O^- ions shows the localization of TPEG SAM on the Au traces. The Au pads and arms where the removal potential was applied are marked by dotted white lines in the upper image to guide the eye. Waveguide labeling is detailed in Fig. 1a.

Table II. Dry resistance values (Ω) measured between two contact pads of waveguides on two dies (labeling as per Fig. 1a).

Waveguide	Die 1	Die 2	Waveguide	Die 1	Die 2
1	886	881	9	920	860
2W	1112	991	10W	920	1122
2E	1021	985	10E	1116	1057
3	817	829	11	881	852
4W	1055	1106	12W	1134	1135
4E	1022	1008	12E	1065	1117
5	919	932	13	859	1118
6W	1034	1032	14W	1129	∞
6E	1081	1032	14E	1047	1005
7	837	799	15	872	833
8W	1118	1013	16W	1055	1029
8E	∞	∞	16E	1107	1034

Interestingly, even though the waveguide 8E and 16W tested open before the electrolysis (see Table II), there was no deterioration of the process. Thus, it is sufficient for only one of the waveguide's pads to make contact with a probe, as long as the waveguide's integrity is maintained.

Based on the intensity of the CH_3O^- ion fragment originating from TPEG, we can see that, as planned, TPEG was desorbed from the west arms of all MZIs on the die and that it stayed behind on all other Au traces. It is therefore verified that our method of removing the TPEG molecules electrochemically from only one Au arm in a single MZI³ works for an array of MZIs.

Die 2 was subjected to the full process cycle A-J (*i.e.*, electrochemical desorption and post-incubation with DDT). ToF-SIMS images of four randomly selected areas are shown in Fig. 7. The left column shows the Au metallization. The middle column depicts, as before, the distribution of TPEG on the Au traces. The right column shows the formation of DDT SAMs on the west arms, where the TPEG had been removed electrochemically (see the lower row in Fig. 6). For DDT ($M = \text{C}_{12}\text{H}_{26}\text{S}$), there are three characteristic ion fragments; *i.e.*, $[\text{M}-\text{H}]^-$ (201.174), $[\text{M}-\text{H}+\text{Au}_2]^-$ (595.108) and $[(\text{M}-\text{H})_2+\text{Au}]^-$ (599.324). We use here the $[(\text{M}-\text{H})_2+\text{Au}]^-$ ion fragment to represent DDT for the purpose of avoiding interference arising for the other two ion fragments, as discussed below.

It is worth noting that, because the Au areas being imaged are small, in order to obtain good signal-to-noise ratios when identifying the presence of DDT molecules, one needs to use as many as *three* characteristic ion fragments associated with the molecule. Shown in Fig. 8 are negative secondary ion mass spectra isolated from four Au pads shown in Figs. 6 and 7 (the identification of the pads is as described in the figure captions). It can be seen that with the $[\text{M}-\text{H}]^-$ and $[\text{M}-\text{H}+\text{Au}_2]^-$ ion fragments (used in previous studies^{17,18}) there

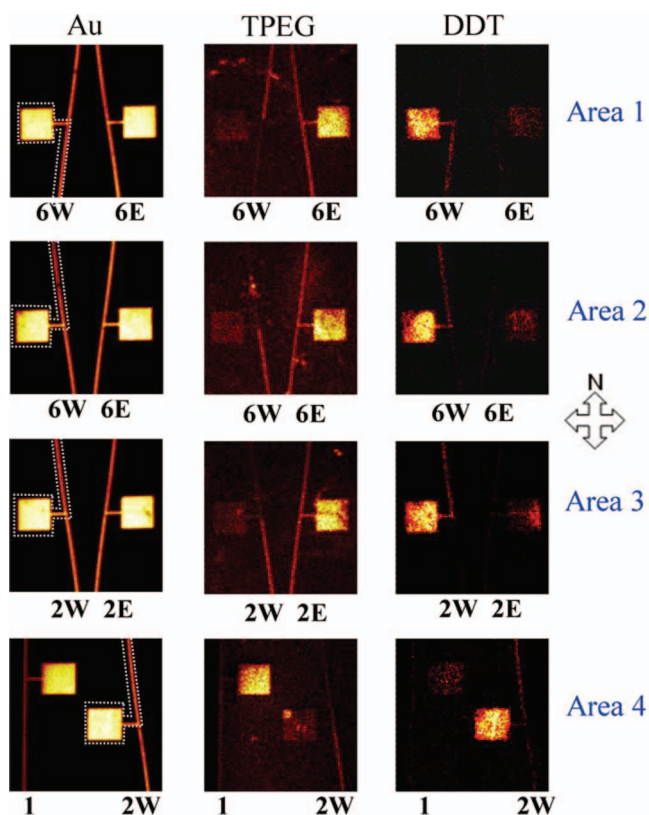


Figure 7. ToF SIMS imaging of Au, TPEG and DDT (columns) for four randomly selected areas ($500 \times 500 \mu\text{m}^2$) of Die 2 subjected to experimental procedure A-J (electrolysis + post-incubation with DDT). Area 1 is situated in a North part of a MZI and Areas 2-4 are in the South part of the die. Au and TPEG are represented by Au_3^- and CH_3O^- , respectively. DDT is represented by the $[(\text{M-H})_2+\text{Au}]^-$, with $\text{M} = \text{C}_{12}\text{H}_{26}\text{S}$. The Au pads and arms where the TPEG SAMs were exchanged with DDT are marked by dotted white lines to guide the eye. Waveguide labeling is detailed in Fig. 1a.

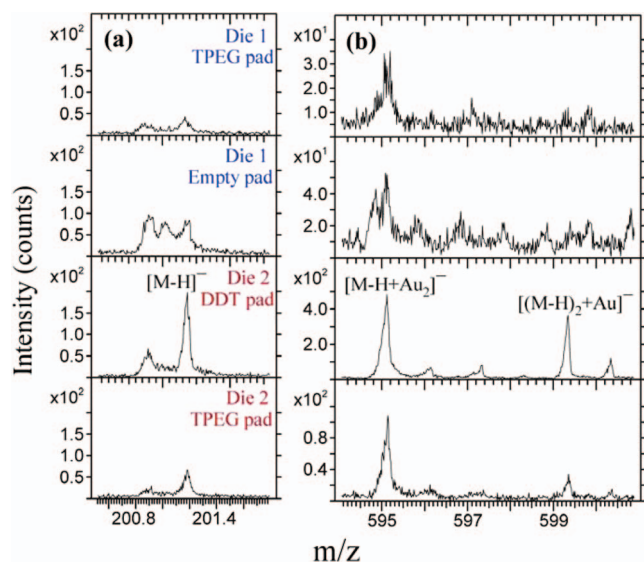


Figure 8. Negative secondary ion mass spectra for: (a) $[\text{M-H}]^-$; and (b) $[\text{M-H}+\text{Au}_2]^-$ and $[(\text{M-H})_2+\text{Au}]^-$. The spectra were isolated from a TPEG pad on Die 1 (1st panel), an empty pad on Die 1 where TPEG was removed (2nd panel), a DDT pad on Die 2 (3rd panel) and a TPEG pad on Die 2 (4th panel). $\text{M} (= \text{C}_{12}\text{H}_{26}\text{S})$ represents the DDT molecule.

is an interference (overlap) with unidentified background peaks. These interfering peaks are normally weak but on small Au features they can become relatively strong and reduce the signal-to-noise ratio. Fortunately the $[(\text{M-H})_2+\text{Au}]^-$ ion fragment is free of such interference, as shown in Fig. 8b. Therefore, this ion was used to represent DDT in the molecular images shown in Fig. 7.

The images in the right column in Fig. 7 prove that the Au areas which lost the TPEG SAM through electrolysis in stages A-I gained a DDT coating post-incubation (stage J) as planned. Also, TPEG-DDT exchange was hardly observed on the other surfaces, in agreement with the conclusion of a previous contact angle study on flat, non-textured Au surfaces¹⁷ which showed that this process is characterized by a long induction time. This is indeed reflected in the mass spectrum in fourth panel in Fig. 8b, where the extremely weak peak of $[(\text{M-H})_2+\text{Au}]^-$ is considered as trace amount of DDT residual.

As demonstrated by our ToF-SIMS analyzes, the selectivity of patterning thiols using our method is excellent, comparable to that of other methods such as micro-contact printing and dip-pen nanolithography.^{19,20} It is worth mentioning that our method is advantageous in selectively patterning different thiols onto narrowly separated, fragile gold structures.

Conclusions

It was shown that electrochemical differentiation of closely-spaced Au features can be scaled to the chip level by using a probe array. The process involves selective electrochemical desorption of a SAM by applying a reductive potential and requires active potential control of all conductive features, both those which are to lose the SAM and those which are to stay unchanged. The post-incubation step deposits another SAM on the liberated Au areas resulting in two chemically differentiated arrays. The process was demonstrated on dies bearing 40 electrically-isolated Au features, connected to 64 contact pads each $100 \times 100 \mu\text{m}^2$ in area, using an array of 64 probes, of which 16 were maintained at a desorbing potential and 48 at a stability potential. ToF-SIMS measurements reveal selective coverage of TPEG or DDT over all features.

Acknowledgments

The authors thank Mr. Jeff Wake of Accuprobe, Inc. for fabrication of the probe array card and the ceramic cell and for related design ideas. They are also grateful to Mr. Hazem Awad for designing and assembling the logical switch matrix and interfacing it with Labview.

References

1. M. Tencer, R. Charbonneau, and P. Berini, *Lab Chip*, **7**, 483 (2007).
2. R. Charbonneau, M. Tencer, N. Lahoud, and P. Berini, *Sensors and Actuators B*, **134**, 455 (2008).
3. M. Tencer, H.-Y. Nie, and P. Berini, *J. Electrochem. Soc.*, **156**, J386 (2009).
4. M. Tencer and P. Berini, *Langmuir*, **24**, 12097 (2008).
5. M. M. Walczak, D. D. Popenoe, R. S. Deinhammer, B. D. Lamp, C. Chung, and M. D. Porter, *Langmuir*, **7**, 2687 (1991).
6. A. Widrig, C. Chung, and M. D. Porter, *J. Electroanal. Chem.*, **310**, 335 (1991).
7. M. M. Walczak, C. A. Alves, B. D. Lamp, and M. D. Porter, *J. Electroanal. Chem.*, **396**, 103 (1995).
8. D.-F. Yang, C. P. Wilde, and M. Morin, *Langmuir*, **12**, 6570 (1996).
9. X. Jiang, R. Ferrigno, M. Mrksich, and G. M. Whitesides, *J. Am. Chem. Soc.*, **125**, 2366 (2003).
10. A. K. Sheridan, P. Ngamukot, P. N. Bartlett, and J. S. Wilkinson, *Sens. Act. B*, **117**, 253 (2006).
11. J. P. Labukas and G. S. Ferguson, *Langmuir*, **27**, 3219 (2011).
12. Y. Xia and G. M. Whitesides, *Angew. Chem. Int. Ed. Engl.*, **37**, 550 (1998).
13. R. D. Piner, J. Zhu, F. Xu, S. Hong, and C. A. Mirkin, *Science*, **283**, 661 (1999).
14. V. S. Golovin and V. G. Zheltov, *Glass and Ceramics*, **34**, 489 (1977).
15. Y. L. Chow, M. M. Elsherbiny, and M. M. A. Salama, *IEEE Proc.-Gener. Transm. Distrib.*, **142**, 653 (1995).
16. M. W. Shinwari, D. Zhitomirsky, I. A. Deen, P. R. Selvaganapathy, M. Jamal Deen, and D. Landheer, *Sensors*, **10**, 1679 (2010).
17. M. Tencer, H.-Y. Nie, and P. Berini, *Surf. Interface Anal.*, **43**, 993 (2011).
18. M. Tencer, H.-Y. Nie, and P. Berini, *Appl. Surf. Sci.*, **257**, 4038 (2011).
19. Y. Xia and G. M. Whitesides, *Angew. Chem., Int. Ed.*, **37**, 550 (1998).
20. R. D. Piner, J. Zhu, F. Xu, S. Hong, and C. A. Mirkin, *Science*, **283**, 661 (1999).